Taylor & Francis
Taylor & Francis Group

Immunological Investigations
A Journal of Molecular and Cellular Immunology

ISSN: (Print) (Online) Journal homepage: www.tandfonline.com/journals/iimm20

Live-Cell Imaging Quantifies Changes in Function and Metabolic NADH Autofluorescence During Macrophage-Mediated Phagocytosis of Tumor Cells

Shelby N. Bess, Matthew J. Igoe & Timothy J. Muldoon

To cite this article: Shelby N. Bess, Matthew J. Igoe & Timothy J. Muldoon (2024) Live-Cell Imaging Quantifies Changes in Function and Metabolic NADH Autofluorescence During Macrophage-Mediated Phagocytosis of Tumor Cells, Immunological Investigations, 53:2, 210-223, DOI: 10.1080/08820139.2023.2284369

To link to this article: https://doi.org/10.1080/08820139.2023.2284369

IMMUNOLOGICAL INVESTIGATIONS
2024, VOL. 53, NO. 2, 210–223
https://doi.org/10.1080/08820139.2023.2284369

Taylor & Francis
Taylor & Francis Group

RESEARCH ARTICLE

Live-Cell Imaging Quantifies Changes in Function and Metabolic NADH Autofluorescence During Macrophage-Mediated Phagocytosis of Tumor Cells

Shelby N. Bess, Matthew J. Igoe, and Timothy J. Muldoon

Department of Biomedical Engineering, University of Arkansas, Fayetteville, Arkansas, USA

ABSTRACT

Background: The immune system has evolved to detect foreign antigens and deliver coordinated responses, while minimizing "friendly fire." Until recently, studies investigating the behavior of immune cells were limited to static *in vitro* measurements. Although static measurements allow for real-time imaging, results are often difficult to translate to an *in vivo* setting. Multiphoton microscopy is an emerging method to capture spatial information on subcellular events and characterize the local microenvironment. Previous studies have shown that multiphoton microscopy can monitor changes in single-cell macrophage heterogeneity during differentiation. Therefore, there is a need to use multiphoton microscopy to monitor molecular interactions during immunological activities like phagocytosis. Here we investigate the correlation between phagocytic function and changes in endogenous optical reporters during phagocytosis.

Methods: *In vitro* autofluorescence imaging of nicotinamide adenine dinucleotide (NADH) and flavin adenine dinucleotide (FAD) was used to detect metabolic changes in macrophages during phagocytosis. More specifically, optical redox ratio, mean NADH fluorescence lifetime and ratio of free to protein-bound NADH were used to quantify changes in metabolism.

Results: Results show that IFN-γ (M1) macrophages showed decreased optical redox ratios and mean NADH lifetime while phagocytosing immunogenic cancer cells compared to metastatic cells. To validate phagocytic function, a fluorescence microscopy-based protocol using a pH-sensitive fluorescent probe was used. Results indicate that M0 and M1 macrophages show similar trends in phagocytic potential.

Conclusion: Overall, this work demonstrates that *in vitro* multiphoton imaging can be used to longitudinally track changes in phagocytosis and endogenous metabolic cofactors.

KEYWORDS
Macrophages; metabolism; phagocytosis; single-cell imaging

Introduction

Immunotherapy is an emerging technique to treat cancer by stimulating or enhancing a patient's immune components to target and inhibit cancer cells, potentially limiting the negative systemic effects associated with untargeted chemotherapy approaches (Bess et al., 2019; Boland & Ma, 2017). Current clinically approved immunotherapy techniques for cancer treatment include monoclonal antibody therapy, adoptive cell transfer (ACT)

CONTACT Timothy J. Muldoon tmuldoon@uark.edu Department of Biomedical Engineering, University of Arkansas, Fayetteville, AR

Supplemental data for this article can be accessed online at https://doi.org/10.1080/08820139.2023.2284369

therapy, cancer vaccines, and cell therapy (Lynch & Murphy, 2016). Among the many types of immunotherapy strategies, monoclonal antibodies have gained the most clinical traction for treating cancer. These antibodies can be divided into two categories: immune checkpoint inhibitors and cytokine-targeted therapy (Noguchi et al., 2013).

Despite successful applications of cancer immunotherapy across a range of human cancers in reducing tumor burden, only a minority of patients experience long-term survival from these therapies (Bess et al., 2019; Boland & Ma, 2017). This likely reflects the highly regulated and complex nature of the immune system (Hegde & Chen, 2020). The immune system requires a series of steps to fulfill the successful immunological elimination of cancer cells. The immune system is also coupled with a series of negative feedback loops, checkpoints, and fail-safes that enable precision control and the ability to shut down an immune response (Hegde & Chen, 2020). The interplay between the human immune system and cancer can lead to a few different outcomes: complete immunological elimination of cancer, uncontrolled cancer growth that can evade an immune response, or a tug-of-war between the two (Hegde & Chen, 2020). One of the key challenges that researchers are focusing on in the field of immunology and cancer biology is understanding the molecular and cellular drivers of immune system escape.

One of the most abundant immune cells within the tumor microenvironment are macrophages. There is growing evidence that specific macrophage populations can influence tumor progression and interfere with cancer treatment (Bejarano et al., 2021; Engblom et al., 2016; Mantovani et al., 2017). Thus, there is significant interest in understanding the biology of macrophages to help researchers and clinicians to overcome the current limitations of cancer therapies. There are several components of macrophage biology that are currently being investigated: 1) exploiting and investigating the functions of the macrophage polarization spectrum, 2) how different macrophage polarization states can contribute to disease suppression or progression, 3) how to promote antitumor immune response while maintaining normal tissue homeostasis, and 4) therapeutic outcomes of macrophage manipulation therapies (Pittet et al., 2022). Macrophages have a variety of origins and functions that are distinct from other immune cells found in solid tumors. Macrophages were first identified as immune cells within the innate immune system that can kill and phagocytose cancer cells, which promote antitumor functions (Evans & Alexander, 1970). However, subsequent studies have shown that macrophages can also promote pro-tumor functions (Qian & Pollard, 2010). More detailed studies have explored the biological complexity of how the tumor microenvironment can convert antitumor phenotype macrophages into pro-tumor macrophages, leading to a decrease in patient survival across many cancer types (Zhang et al., 2012).

Typically, macrophages that comprise the immune system are constantly patrolling the body looking for pathogens (Dzhagalov et al., 2012). The immune system has evolved to detect foreign antigens and deliver sets of coordinated responses (i.e., cytokine delivery, antibody production, and development of immunological memory) while minimizing "friendly fire" that could result in autoimmune disease (Matheu et al., 2011). Until recently, studies were limited to static measurements in cell populations in living animals or to *in vitro* experiments using individual cells in artificial environments. Even though the latter approach allows for real-time imaging, the results were often difficult to relate in the *in vivo* setting (Matheu et al., 2011). Live-cell multiphoton microscopy is an emerging method that is being applied to capture the dynamic nature of immune cell behavior including immune

cell activation (Dzhagalov et al., 2012; Matheu et al., 2011). More specifically, multiphoton microscopy can quantify the endogenous autofluorescence of the metabolic coenzymes NADH and FAD, which are used in several metabolic processes. Nicotinamide adenine dinucleotide (NAD), serves as a major metabolic electron carrier and can exist in a reduced (NADH), oxidized (NAD+), or phosphorylated (NAD(P)H) forms (Jones et al., 2018). Similarly, flavin adenine dinucleotide (FAD) is also a metabolic electron carrier that can exist in a reduced ($FADH_2$) or oxidized (FAD) form. Out of all the redox cofactors, NADH, NAD(P)H, and FAD are autofluorescent, with NADH exhibiting the highest fluorescence intensity (Jones et al., 2018; Miksa et al., 2009). The quantification of the fluorescence signals of these cofactors can provide an estimate of metabolic activity because metabolic potential coincides with the ratio of reduced and oxidized metabolic substrates. The use of high-resolution microscopy techniques enables an increased understanding of the heterogeneity of dynamic changes in redox states within cells and provides insight previously unachievable through other methods. However, one of the major challenges with intensity-based measurements is that the quantum yield of NADH and FAD is significantly lower than that of commonly used fluorophores such as fluorescein. These relatively weak fluorescence measurements can be difficult due to hemodynamic changes within the tissue (especially in tissues where collagen autofluorescence is present), which can affect intensity-based measurements (Jones et al., 2018; Minhas et al., 2019). Fluorescence lifetime imaging (FLIM) can overcome these challenges due to its ability to extract metabolic information at one excitation wavelength and is sensitive to the molecular microenvironment. FLIM is typically used to determine the binding fraction of fluorophores based on their lifetimes in unbound and protein-bound states (Jones et al., 2018; Minhas et al., 2019). NAD(P)H FLIM measurements can be an alternative to the optical redox ratio. NADH transfers electrons through the binding to a variety of dehydrogenases and depending on whether the molecule is free or protein-bound, it can affect its fluorescence quantum yield (Jones et al., 2018). Protein-bound NAD(P)H has a higher quantum yield than free NAD(P)H, which emits a higher intensity. Spatially and temporally resolved measurements of NAD(P)H are typically performed using time-correlated single-photon counting (TSCPC). This technique quantifies fluorescence lifetime by measuring the time between a laser pulse and the detection of a single emitted photon. Over many photons, a histogram can be fitted to a decay curve to estimate the characteristics of this decay. Biexponential models are commonly fitted to the histogram at each pixel to obtain the decay curve $I(t) = I_0(A_1 e^{\left(-t/\tau_1\right)} + A_2 e^{\left(-t/\tau_2\right)}$, where I_0 is the initial fluorescence intensity, τ_1 and τ_2 are the short and long lifetime components, respectively, and A_1 and A_2 are their respective relative contributions to the total fluorescence. The ratio of A_1/A_2 is frequently used as a summary statistic to describe the lifetime decay of NADH. This type of microscopy allows for the visualization of migration behavior, signaling, cell death, cell-cell interactions, cell-microbe interactions, relocalization of proteins, etc (Dzhagalov et al., 2012; Matheu et al., 2011). Over time, this technique has evolved to address advanced immunological questions and is now routinely performed in a variety of tissues such as lymph nodes, skin, spinal cord, bone marrow, and liver (Matheu et al., 2011). For example, researchers have used intravital imaging to investigate how the immune system is activated in response to inflammation within the respiratory system (Kim et al., 2019). Even though, these researchers were able to visualize the movement of leukocytes within the native

environment, immune cell populations of interest were labeled with fluorescent proteins, which can interfere with the autofluorescence of endogenous fluorophores that can provide insight into migration, metabolism, and other subcellular events (Wizenty et al., 2020). Recent immunological studies are now moving towards single-cell methods. The direct imaging of cells undergoing biological activities such as activation provides important spatial information that can help describe subcellular events and/or characterize the local microenvironment. Previous studies have shown that autofluorescence imaging using multiphoton microscopy can monitor changes in single-cell macrophage heterogeneity during polarization and migration within a simulated three-dimensional model of a tumor microenvironment (Heaster et al., 2020). Even though single-cell imaging is beginning to enter the immunology field, traditional methods such as intravital imaging (imaging of cells within a live animal through an imaging window) and flow cytometry are still the most common methodologies to investigate immunological processes. These methodologies can only provide limited insight since they do not account for a spectrum (i.e., cells undergoing different stages of differentiation) of cells within a phenotypic cellular population. Therefore, there is a need to investigate the immune cell landscape at the single-cell level to understand the molecular interactions between immune cells and their surrounding environment. Here, we use autofluorescence imaging of metabolic co-factors (NADH and FAD) in macrophage cytoplasm to investigate the metabolic and functional changes in active macrophages as they perform tumor cell phagocytosis, while using a traditional fluorescence microscopy to verify the longitudinal, single-cell changes in macrophage function.

Materials and methods

Macrophage and cancer cell culture

Murine RAW 264.7 (ATCC©, TIB-71™) macrophages were maintained in Roswell Park Memorial Institute (RPMI)-1640 medium (Invitrogen™, 10104-CV) with 10% fetal bovine serum (FBS) (ATCC©, 30–2020™) and 1% gentamicin (Invitrogen™, 15710064). Cells were grown to ~ 80% confluency prior to all experiments and passage numbers remained under five. RAW 264.7 macrophages were seeded at a density of 1×10^6 cells/mL in a 35 mm MatTek© culture dish at 37°C and 5% CO_2 24 hours prior to cytokine stimulation to allow for cell adhesion to the culture dish. Macrophages were polarized towards M0, or M1 with the following: M0 (RPMI-1640 medium only) or M1 (RPMI-1640 medium supplemented with 10 ng/mL IFN-γ (R&D Systems, ®485-MI-100). Macrophages remained in their cytokine-supplemented medium for 72 hours to allow for complete differentiation into their respective phenotypes. Murine CT26 (ATCC©, CRL-2638) colorectal adenocarcinoma and 4T1 (ATCC©, CRL-2539) metastatic breast cancer cells were maintained in RPMI-1640 medium supplemented with 10% FBS and 1% gentamicin. Cancer cells were grown to ~ 80% confluency prior to all experiments and passage numbers remained under 20. Prior to all experiments, the CT26 and 4T1 cells were brought to a concentration of 2×10^6 cells/mL. Cancer cell lines were chosen according to their relative expression of CD47 and PD-L1. The relative CD47 and PD-L1 expressions of these cell lines are shown in Table 1.

Table 1. Surface CD47 and PD-L1 expression of CT26 and 4T1 cell lines (Lian et al., 2019).

Cell Lines	CD47 Expression (%)	PD-L1 Expression (%)
CT26	99.8	78.2
4T1	99.7	91.9

Phagocytosis assay

An adapted protocol (Lian et al., 2019) was used to determine the degree of phagocytosis of cancer cells using pHrodo-succinimidyl ester (pHrodo-SE). A summary of the protocol is shown in Figure 1. Briefly, CT26 or 4T1 cells were harvested at 2×10^6 cells/mL and stained with 120 ng/mL of pHrodo-SE (Invitrogen™, P36600) for 30 minutes. Cytokine-stimulated macrophages were washed in phosphate-buffered saline (PBS) prior to labeling with 1 μM 5-chloromethylfluorescein diacetate (CMFDA, Invitrogen™ CellTracker™, C2925) for 30 minutes. CT26 or 4T1 cells were then washed with PBS and resuspended in RPMI-1640 medium. Cancer cells were then added to the macrophages and allowed to incubate at 37°C and 5% CO_2 for 30 minutes prior to imaging. After co-incubation, the dish of cells was moved to a microincubator located inside a confocal microscope (Olympus Fluoview FV10i-LiV) with a 60X (1.2 N.A., water-immersion) objective with controllable temperature and humidified gas delivery (5% CO2). Images (1024 × 1024) were captured at an 8-bit depth with a field of view of 0.223 × 0.223 μm. The degree of phagocytosis of cancer cells was measured at 15-minute intervals (frame time of 26 seconds) over a two-hour period

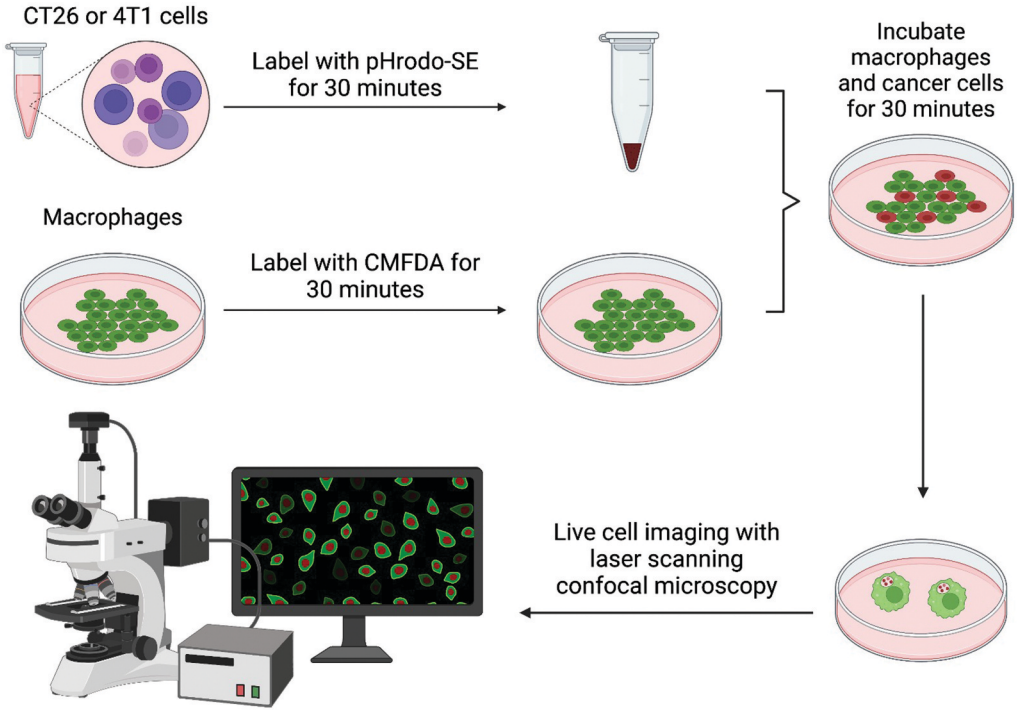

Figure 1. Schematic of live-cell phagocytosis assay. Figure was created with BioRender.

(Olympus) and analyzed by randomly selecting six microscopic fields of view. Two values were calculated: % Phagocytosis and Phagocytosis Index. Phagocytosis percentage (%) was calculated with the following formula: number of CMFDA+ RAW 264.7 macrophage phagocytosing CT26 or 4T1 cancer cells/total number of CMFDA+ RAW 264.7 macrophages x 100. Phagocytosis Index was calculated with the following formula: number of engulfed pHrodo-SE+ CT26 or 4T1 cancer cells/total number of CMFDA+ RAW 264.7 macrophages.

Live cell metabolic imaging of macrophage-mediated phagocytosis of cancer cells

Prior to imaging, cancer cells will be brought to a single-cell suspension at a density of 2 million cells/mL and stained with pHrodo-SE at a final concentration of 120 ng/mL. The 1 mL suspension of the pHrodo-SE-stained cancer cells was added to the macrophages (unstained) and placed in the incubator for 30 minutes prior to imaging. Prior to imaging, cells were moved to a microincubator (Warner Instruments, DH-35iL) with controllable temperature and humidified gas delivery (5% CO2). A custom inverted multiphoton imaging system (Bruker custom system) equipped with an Ultrafast Ti:Sapphire (Mai Tai HP, Spectra Physics, Inc.) via a (60×/1.2NA) water immersion objective (Olympus) and four close-proximity, high-efficiency GaAsP detectors using Prairie View 5.5. NAD(P)H fluorescence was captured with a 460 (±20) nm bandpass filter at 755 nm excitation. PMT gains were as follows for NAD(P)H fluorescence: PMT 1 (Red) = 800, PMT (Green) = 800, PMT 3 (Blue) = 850, PMT 4 (UV) = 800. FAD fluorescence with a 525 (±25) nm bandpass filter at 855 nm excitation. PMT gains were as follows for FAD fluorescence: PMT 1 (Red) = 800, PMT (Green) = 850, PMT 3 (Blue) = 800, PMT 4 (UV) = 800. Detection of pHrodo-SE-stained cancer cells were captured with a <430 nm band pass filter at 1000 nm excitation. PMT gains were as follows for pHrodo-SE detection: PMT 1 (Red) = 850, PMT (Green) = 800, PMT 3 (Blue) = 800, PMT 4 (UV) = 800. NAD(P)H and FAD fluorescence along with pHrodo-SE detection was normalized by PMT gain and laser power (~2 mW), with PMT gain normalized to fluorescein concentrations (0.1 μM to 20 μM in Tris Buffer of pH 8) as in previous studies (Viola et al., 2019). PMT gain and laser power were kept constant, and laser power was read after each imaging session. Images (1024 × 1024) were captured at a 16-bit depth with a field of view of 181.5 × 181.5 μm and a pixel size of 0.117 × 0.117 μm. Average dwell time for image acquisition was 10 μs. Once the images have been acquired, a binary mask of the pHrodo-SE images was created to assess for engulfed cancer cells. If cancer cells were detected, the binary mask was overlayed with binary masks of NADH and FAD images to determine the number of macrophages undergoing phagocytosis. Once that was determined, the binary mask of the pHrodo-SE images was subtracted from the binary masks of the NADH and FAD images to capture the optical metrics of only the cytoplasm of active macrophages. After that, pixel-by-pixel optical redox ratios and A1/A2 ratios were calculated for individual phagocytes.

Data analysis and statistics

Pixel-wise calculations of the optical redox ratio were computed in a custom MATLAB script after normalizing fluorescent intensities based on the day-to-day variability of the lasers. The resulting redox ratios were assigned to a jet color map within MATLAB with

upper and lower limits (0 and 1). Fluorescence lifetime images were analyzed with SPCImage 8.3 (Becker and Hickl GmbH, Berlin, Germany). An incomplete multiexponential model was used, with lifetime images spatially binned to obtain pixel photon counts to a minimum of 10,000. Fits were generated using the instrument response function (IRF), measured using urea crystal standards, with a biexponential decay model to separate the short (A1) and long (A2) components of free and protein bound NADH. Images with χ^2 values between 1.0 and 1.4 were appropriately fit (Supplemental Information Figure S1). A mixed effects, one-way analysis of variance (ANOVA), and a Tukey's honestly significant difference (HSD) test were used to evaluate statistical significance between specific experimental groups. A p-value of $< .05$ is considered statistically significant (Quinn et al., 2013).

Results

Autofluorescence metabolic imaging shows changes in macrophage cytoplasmic metabolism during cancer cell phagocytosis of varying CD47 and PD-L1 expression

Actively phagocytosing macrophages were detected using binary masks of pHrodo-SE and NADH autofluorescence channels and overlaid. As shown in Figure 2, the optical redox ratio of the M0 macrophage cytoplasm during phagocytosis was higher during active phagocytosis of

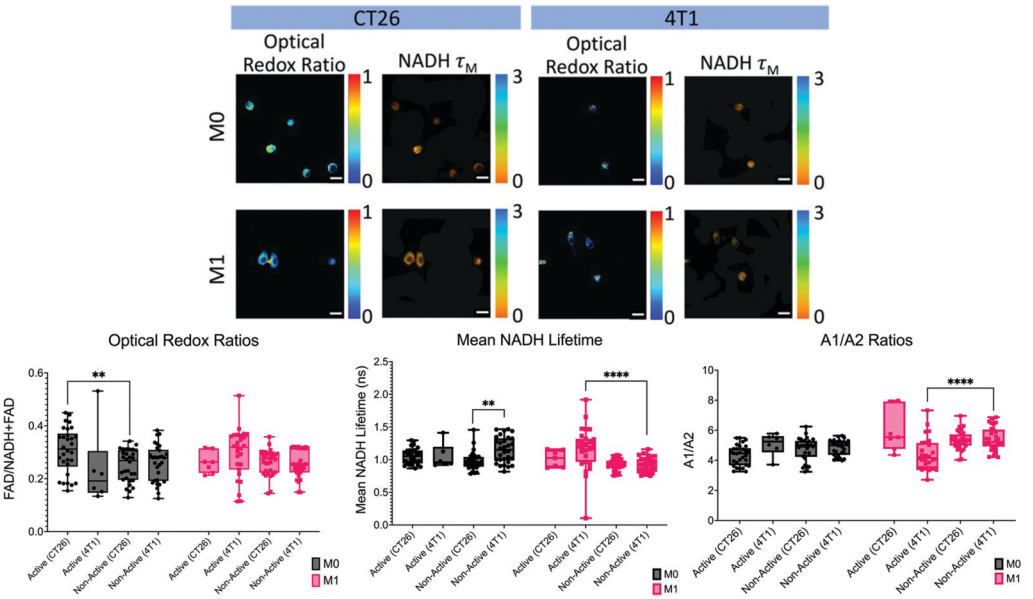

Figure 2. Autofluorescence imaging of NADH and FAD can detect changes in macrophage cytoplasmic metabolism during macrophage-mediated phagocytosis. Top: Representative images of optical redox ratio and mean NADH lifetime of actively functioning macrophages phagocytosing CT26 or 4T1 cancer cells as determined by using a binary mask of the pHrodo-SE images was created to assess for engulfed cancer cells. If cancer cells were detected, the binary mask was overlayed with binary masks of NADH and FAD images to determine which macrophages were performing phagocytosis. Bottom: Plots comparing optical redox ratios, mean NADH lifetime and A1/A2 ratios in active vs non-active macrophages. ** $p \leq .01$ **** $p \leq .0001$. Scale bars are 20 µm. All plots were created in GraphPad Prism®.

CT26 cells (0.307 ± 0.087) compared to 4T1 cells (0.238 ± 0.149) while A1/A2 ratio was lower when phagocytosing CT26 (4.342 ± 0.674) vs 4T1 (5.061 ± 0.747). No distinct changes in mean NADH lifetime were observed for M0 macrophages regardless of which cancer cell line they were phagocytosing. Significant differences were observed when comparing the optical redox ratios of non-actively phagocytosing M0 macrophages ($p = .0010$) for CT26 cells. M1 macrophages showed a slightly higher optical redox ratio when phagocytosing 4T1 cells (0.296 ± 0.092) compared to CT26 cells (0.263 ± 0.041). No significant differences were observed when comparing actively phagocytosing and non-phagocytosing M1 macrophages. M1 macrophages also showed a slightly higher mean NADH lifetime when phagocytosing 4T1 cells (1.174 ± 0.333 ns) compared to CT26 cells (1.015 ± 0.127 ns). Again, no significant differences were observed when comparing actively phagocytosing and non-phagocytosing macrophages of CT26 cells. A significant difference was observed when comparing actively phagocytosing and non-phagocytosing macrophages of 4T1 cells in M1 macrophages ($p < .0001$). M1 macrophages phagocytosing CT26 cells showed a higher A1/A2 ratio (5.965 ± 1.436) when compared to M1 macrophages phagocytosing 4T1 cells (4.424 ± 1.068) and when compared to non-actively phagocytosing macrophages (CT26: 5.332 ± 0.629 and 4T1: 5.416 ± 0.775). Major significant differences were observed when comparing actively phagocytosing and non-phagocytosing of 4T1 cells in M1 macrophages ($p < .0001$). Overall, autofluorescence imaging of metabolic co-factors was able to show endogenous changes in the cytoplasmic metabolism of macrophages as they performed phagocytosis of cancer cells.

M0 and M1 macrophages show similar trends in phagocytic function of cancer cells

To analyze the phagocytic function of the cytokine-stimulated macrophages, an image-based phagocytosis assay was used to quantitatively measure the engulfment of cancer cells over time. Cells stained with pHrodo-SE will emit a low (non-engulfed) or bright fluorescence (engulfed within a phagolysosome) depending on the pH in the surrounding microenvironment. Here, we compared the phagocytic function of this macrophage model using CT26 or 4T1 cancer cells (Figure 3a). M0 macrophages and M1 macrophages showed similar trends in % phagocytosis and phagocytosis index. M0 macrophages showed approximately 39.302 ± 5.015% phagocytosis for the first 60 minutes, while M1 macrophages showed 34.843 ± 14.897% phagocytosis when phagocytosing CT26 cells. Interestingly, after 30 minutes, M0 and M1 macrophages kept a consistent % phagocytosis when phagocytosing 4T1 cells (M0: 33.381 ± 7.328; M1: 25.031 ± 14.010) (Figure 3b). As shown in Figure 3c, M0 and M1 macrophages showed similar values in phagocytosis index (M0: 1.131 ± 0.318; M1: 1.037 ± 0.553) during the first 45 minutes of the assay before tapering off. Again, the phagocytosis index of M0 and M1 macrophages phagocytosing 4T1 cells increased to similar values to that of CT26 after 60 minutes (M0: 1.098 ± 0.261; M1: 0.928 ± 0.593). Overall, a fluorescence microscopy-based phagocytosis was able to detect and longitudinally track macrophage-mediated phagocytosis of cancer cells at the single-cell level.

Modest correlations between phagocytic function and optical metabolic metrics were observed

Pearson correlations and linear regressions were used to investigate any correlations between the acute changes in intracellular metabolic co-factors (NADH and FAD) with

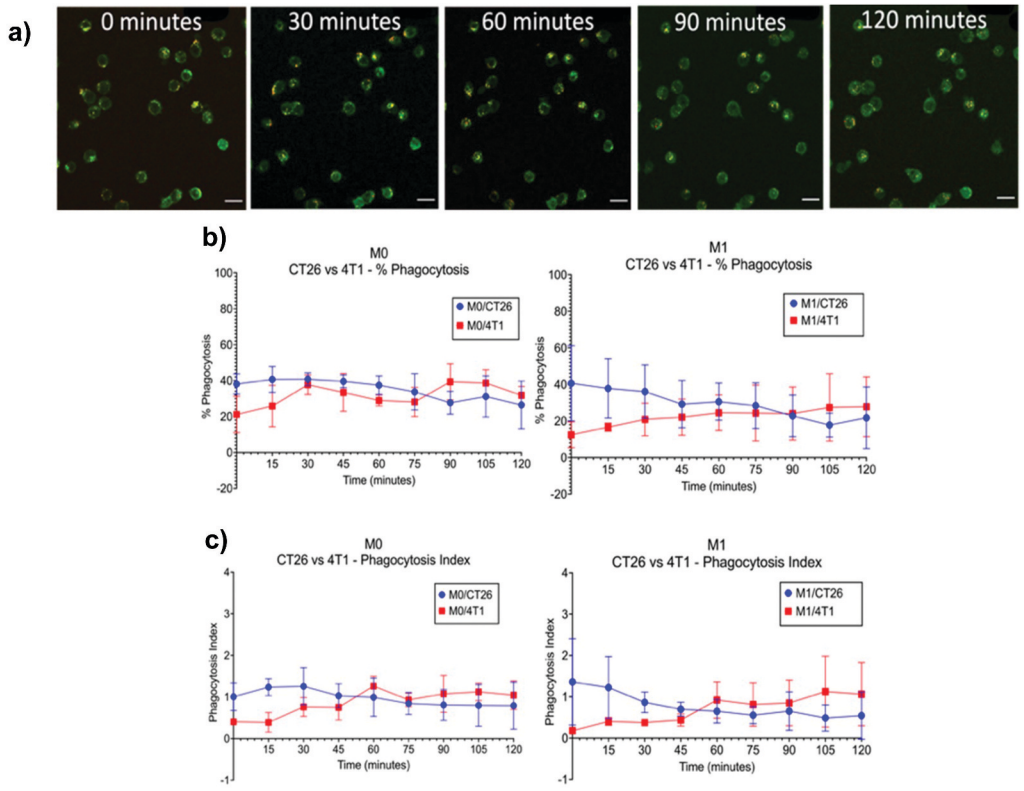

Figure 3. M0 and M1 macrophages show similar trends in phagocytic function. a) Representative fluorescence images of CMFDA+ macrophages (green) engulfing pHrodo-SE positive cancer (red) cells at 30-minute intervals over a two-hour period. b) Trends in % phagocytosis over a two-hour period. c) Trends in phagocytosis index over a two-hour period. Scale bars are 10μm. All plots were created in GraphPad Prism®.

macrophage phagocytic function. As shown in Figure 4 and Supplemental Information Table S1, no significant correlation was observed when comparing % phagocytosis (R^2 = −0.044) and phagocytosis index (R^2 = −0.0205) with optical redox ratio (Figure 4a,d). Low, but significant negative correlations were observed when comparing % phagocytosis (R^2 = −0.2937, p = .017) and phagocytosis index (R^2 = −0.248, p = .045) to mean NADH lifetime (Figure 4b,e). Even though the correlations were not significant, there was a low positive correlation between % phagocytosis and A1/A2 ratio (R^2 = 0.166, p = .184). Interestingly, there was a low negative correlation between the phagocytosis index and A1/A2 ratio (R^2 = −0.161, p = .196). Overall, results indicate that there could be a weak correlation that can relate phagocytic function to changes in intracellular metabolic co-factors.

Discussion

Autofluorescence imaging of the intensities and lifetimes of metabolic co-factors (NADH and FAD) is an emerging methodology in the immunology field that allows for longitudinal monitoring of immune cell metabolism and function *in vitro*. The reduced form of NADH

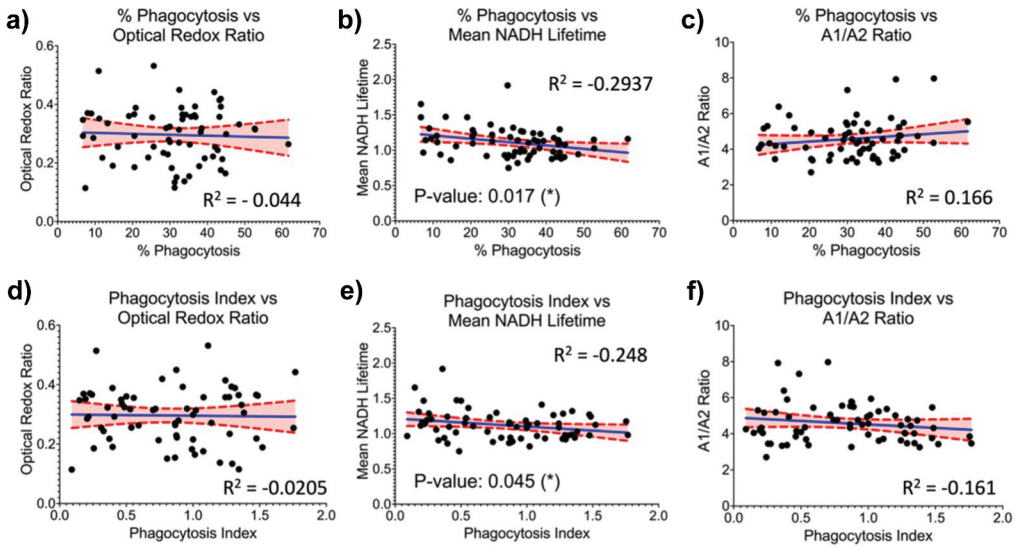

Figure 4. Correlations in phagocytic function and optical metabolic metrics. Top: correlations between % phagocytosis and a) optical redox ratio, b) mean NADH lifetime and c) A1/A2 ratio. Bottom: Correlations between phagocytosis index and d) optical redox ratio, e) mean NADH lifetime and f) A1/A2 ratio. Red dotted lines indicate the upper and lower 95% confidence limits. Red shaded regions indicate the 95% confidence interval. Bolded blue lines indicate the line of best fit.

and oxidized form of FAD are endogenous metabolic coenzymes that are autofluorescent which allows one to use their intensities to determine the optical redox ratio, which can provide insight into the oxidation-reduction state of a cell as it performs an intended function, such as phagocytosis of tumor cells (Miskolci et al., 2022). In this study, we compared the cytoplasmic metabolism of M0 and M1 macrophages as they were actively performing phagocytosis of two cancer cell lines (CT26 and 4T1) that were exogenously labeled with a pH-sensitive probe. As expected, M1 macrophages showed a decrease in optical redox ratio as they actively phagocytose immunogenic cancer cells (CT26) compared to a metastatic cell line (4T1). Interestingly, M0 macrophages showed the opposite trend where there was an increase in optical redox ratio as they phagocytosed immunogenic cancer cells (CT26) compared to a metastatic cell line (4T1). FLIM is also highly applicable to the immunology field because of its ability to provide additional biological information through the distinction of free vs protein-bound states, while being independent on the cellular concentration of metabolic coenzymes (Kolenc & Quinn, 2019; Miskolci et al., 2022) Here, our results indicate that there were no distinct changes in mean NADH lifetime and A1/A2 ratio with M0 macrophages during phagocytosis. M1 macrophages phagocytosing CT26 cells showed a lower mean NADH lifetime and a higher A1/A2 ratio value compared to the 4T1 cells. Future work could include using an optical imaging system that can simultaneously collect NADH and FAD autofluorescence along with the detection of pH-sensitive fluorescent probes to ensure that image pixels are aligned with each other and to prevent crosstalk between different wavelengths to ensure that the detection of an engulfed cancer cell is accurately detected. Overall, autofluorescence imaging along with the addition of a pH-sensitive fluorescent probe can be a reliable method to determine the

cytoplasmic metabolism of macrophages at the single-cell level as they perform tumor cell phagocytosis.

Traditional methods (i.e., flow cytometry) have been used to assess cancer cell engulfment through the utilization of fluorescent pH-sensitive dyes (Lian et al., 2019; Miksa et al., 2009). However, flow-cytometry-based approaches provide limited information on the single-cell changes in phagocytosis and can overestimate the potential of tumor cell phagocytosis due to bulk aggregation and the inappropriate detection of intercellular binding. Therefore, an adapted protocol for detecting tumor cell phagocytosis through confocal microscopy using pHrodo-SE dye was used to visualize the detection of phagocytosis at the single cell level. pHrodo-SE dye was utilized for tumor cell labeling due to its ability to react with primary amines to yield covalently linked pH proves, leading to an increase in fluorescence as the environmental pH of the phagolysosome becomes more acidic (Miksa et al., 2009). This approach allows the cancer cells to easily distinguish engulfed cancer cells from those that are adhered to the outer surface of macrophages. Therefore, this technique allows for easier quantification of tumor cell phagocytosis at the single-cell level. Using this technique, our results show that inactivated M0 macrophages and IFN-γ stimulated M1 macrophages show a similar potential in the percentage of phagocytosing macrophages. When comparing the phagocytic ability of our macrophage model to tumor cells of varying CD47 and PD-L1 surface expression, both the M0 and M1 macrophages show a higher percentage of phagocytosis with immunogenic CT26 cells within the first 60 minutes compared to metastatic 4T1 cells. Interestingly, after the first 60 minutes, both the M0 and M1 show a higher percentage of phagocytosis with metastatic 4T1 cells compared to immunogenic CT26 cells. Our results also indicate little variation in the percentage of phagocytosis and the phagocytosis index. During macrophage phagocytosis, as described in a study by Richards et al, there are two distinct stages during the engulfment of particles during the phagocytosis process [Richards et al, 2014]. The first stage of engulfment is relatively slow. Once a foreign particle/cell has been approximately half-engulfed by the macrophage, the rate of engulfment increases dramatically. During our study, the little variation in % phagocytosis and phagocytosis index over the selection two-hour period, could be occurring during the first stage of engulfment. The chosen imaging methodology is looking at the macrophage population (M0 or M1) as a whole and could be further improved on by investigating the changes in engulfment (based on pHrodo-SE intensity) of a single macrophage over time. Other limitations to this approach include ensuring the samples are maintained under the correct environmental conditions during imaging and avoiding photobleaching of fluorescent markers over time since excitation light can damage cellular components causing impairment in physiology. Overall, the use of a fluorescence microscopy approach to longitudinally track macrophage-mediated phagocytosis can be useful in determining the efficacy of various immunotherapeutic approaches.

Studies are now beginning to address the role of the redox and metabolic status of macrophages with functional response. For example, the investigation of the oxidized and reduced forms of NADH and FAD has been demonstrated in M1-polarized macrophage functions such as TNF-α production (Al-Shabany et al., 2016), oxidative phosphorylation (Minhas et al., 2019), and cellular adhesion for phagocytosis (Venter et al., 2014). However, there are currently no studies investigating the correlations in the phagocytic capacity of macrophages with the changes in metabolism that occur during tumor cell phagocytosis. Using linear regression and Pearson's correlations, we noticed

that there was low, but significant correlations when comparing % phagocytosis and phagocytosis index with mean NADH lifetime, meaning that as phagocytic function increases, the mean NADH lifetime decreases. These results coincide with previous literature stating that the rate of glycolysis is increased during phagocytosis (Viola et al., 2019). However, as previous mentioned, our results could be occurring during the first stage of engulfment and not the whole phagocytosis process. More studies should be performed to investigate the changes in metabolism during the engulfment and the digestion of the foreign particle/body. Overall, the findings in this work suggest that not only can phagocytic function be longitudinally quantified, but acute changes in endogenous metabolic cofactors can also be quantified and correlated.

Disclosure statement

No potential conflict of interest was reported by the author(s).

Funding

This work was supported by the National Science Foundation (CBET 1751554), the National Institutes of Health, Arkansas Integrative Metabolic Research Center (5P20GM139768-02), and the Arkansas Biosciences Institute. Any opinions, findings, and conclusions or recommendations expressed in this material are those of the authors and do not necessarily reflect the views of the acknowledged funding agencies.

Data availability statement

The datasets generated and/or analyzed during the current study are available in the figshare repository located at this link: https://figshare.com/projects/Live-cell_NADH_autofluorescence_during_phagocytosis/163321

References

Al-Shabany, A. J., Moody, A. J., Foey, A. D., & Billington, R. A. (2016). Intracellular NAD+ levels are associated with LPS-induced TNF-α release in pro-inflammatory macrophages. *Bioscience Reports*, *36*(1), e00301. https://doi.org/10.1042/BSR20150247

Bejarano, L., Jordão, M., & Joyce, J. A. (2021). Therapeutic targeting of the tumor microenvironment. *Cancer Discovery*, *11*(4), 933–959. https://doi.org/10.1158/2159-8290.CD-20-1808

Bess, S. N., Greening, G. J., & Muldoon, T. J. (2019). Efficacy and clinical monitoring strategies for immune checkpoint inhibitors and targeted cytokine immunotherapy for locally advanced and metastatic colorectal cancer. *Cytokine & Growth Factor Reviews*, *49*, 1–9. https://doi.org/10.1016/j.cytogfr.2019.10.002

Boland, P. M., & Ma, W. W. (2017). Immunotherapy for colorectal cancer. *Cancers*, *9*(5), 50. https://doi.org/10.3390/cancers9050050

Dzhagalov, I. L., Melichar, H. J., Ross, J. O., Herzmark, P., & Robey, E. A. (2012). Two-photon imaging of the immune system. *Current Protocols in Cytometry, Chapter 12*, *60*(1), Unit12.26. https://doi.org/10.1002/0471142956.cy1226s60

Engblom, C., Pfirschke, C., & Pittet, M. J. (2016). The role of myeloid cells in cancer therapies. *Nature Reviews Cancer*, *16*(7), 447–462. https://doi.org/10.1038/nrc.2016.54

Evans, R., & Alexander, P. (1970). Cooperation of immune lymphoid cells with macrophages in tumour immunity. *Nature*, *228*(5272), 620–622. https://doi.org/10.1038/228620a0

Heaster, T. M., Humayun, M., Yu, J., Beebe, D. J., & Skala, M. C. (2020). Autofluorescence imaging of 3D tumor-macrophage microscale cultures resolves spatial and temporal dynamics of macrophage metabolism. *Cancer Research*, *80*(23), 5408–5423. https://doi.org/10.1158/0008-5472.CAN-20-0831

Hegde, P. S., & Chen, D. S. (2020). Top 10 challenges in cancer immunotherapy. *Immunity*, *52*(1), 17–35. https://doi.org/10.1016/j.immuni.2019.12.011

Jones, J. D., Ramser, H. E., Woessner, A. E., & Quinn, K. P. (2018). *In vivo* multiphoton microscopy detects longitudinal metabolic changes associated with delayed skin wound healing. *Communications Biology*, *1*(1), 198. https://doi.org/10.1038/s42003-018-0206-4

Kim, Y. M., Jeong, S., Choe, Y. H., & Hyun, Y. M. (2019). Two-photon intravital imaging of leukocyte migration during inflammation in the respiratory system. *Acute and Critical Care*, *34*(2), 101–107. https://doi.org/10.4266/acc.2019.00542

Kolenc, O. I., & Quinn, K. P. (2019). Evaluating cell metabolism through autofluorescence imaging of NAD(P)H and FAD. *Antioxidants & Redox Signaling*, *30*(6), 875–889. https://doi.org/10.1089/ars.2017.7451

Lian, S., Xie, R., Ye, Y., Xie, X., Li, S., Lu, Y., Li, B., Cheng, Y., Katanaev, V. L., & Jia, L. (2019). Simultaneous blocking of CD47 and PD-L1 increases innate and adaptive cancer immune responses and cytokine release. *E Bio Medicine*, *42*, 281–295. https://doi.org/10.1016/j.ebiom.2019.03.018

Lynch, D., & Murphy, A. (2016). The emerging role of immunotherapy in colorectal cancer. *Annals of Translational Medicine*, *4*(16), 305. https://doi.org/10.21037/atm.2016.08.29

Mantovani, A., Marchesi, F., Malesci, A., Laghi, L., & Allavena, P. (2017). Tumour-associated macrophages as treatment targets in oncology. *Nature Reviews Clinical Oncology*, *14*(7), 399–416. https://doi.org/10.1038/nrclinonc.2016.217

Matheu, M. P., Cahalan, M. D., & Parker, I. (2011). Immunoimaging: Studying immune system dynamics using two-photon microscopy. *Cold Spring Harbor Protocols*, *2011*(2), db.top99. https://doi.org/10.1101/pdb.top99

Miksa, M., Komura, H., Wu, R., Shah, K. G., & Wang, P. (2009). A novel method to determine the engulfment of apoptotic cells by macrophages using pHrodo succinimidyl ester. *Journal of Immunological Methods*, *342*(1–2), 71–77. https://doi.org/10.1016/j.jim.2008.11.019

Minhas, P. S., Liu, L., Moon, P. K., Joshi, A. U., Dove, C., Mhatre, S., Contrepois, K., Wang, Q., Lee, B. A., Coronado, M., Bernstein, D., Snyder, M. P., Migaud, M., Majeti, R., Mochly-Rosen, D., Rabinowitz, J. D., & Andreasson, K. I. (2019). Macrophage de novo NAD^+ synthesis specifies immune function in aging and inflammation. *Nature Immunology*, *20*(1), 50–63. https://doi.org/10.1038/s41590-018-0255-3

Miskolci, V., Tweed, K. E., Lasarev, M. R., Britt, E. C., Walsh, A. J., Zimmerman, L. J., McDougal, C. E., Cronan, M. R., Fan, J., Sauer, J. D., Skala, M. C., & Huttenlocher, A. (2022). In vivo fluorescence lifetime imaging of macrophage intracellular metabolism during wound responses in zebrafish. *eLife*, *11*, e66080. https://doi.org/10.7554/eLife.66080

Noguchi, T., Ritter, G., & Nishikawa, H. (2013). Antibody-based therapy in colorectal cancer. *Immunotherapy*, *5*(5), 533–545. https://doi.org/10.2217/imt.13.35

Pittet, M. J., Michielin, O., & Migliorini, D. (2022). Clinical relevance of tumour-associated macrophages. *Nature Reviews Clinical Oncology*. Advance online publication. https://doi.org/10.1038/s41571-022-00620-6

Qian, B. Z., & Pollard, J. W. (2010). Macrophage diversity enhances tumor progression and metastasis. *Cell*, *141*(1), 39–51. https://doi.org/10.1016/j.cell.2010.03.014

Quinn, K. P., Sridharan, G. V., Hayden, R. S., Kaplan, D. L., Lee, K., & Georgakoudi, I. (2013). Quantitative metabolic imaging using endogenous fluorescence to detect stem cell differentiation. *Scientific Reports*, *3*(1), 3432. https://doi.org/10.1038/srep03432

Venter, G., Oerlemans, F. T., Willemse, M., Wijers, M., Fransen, J. A., Wieringa, B., & Dzeja, P. (2014). NAMPT-mediated salvage synthesis of NAD+ controls morphofunctional changes of macrophages. *PloS One*, *9*(5), e97378. https://doi.org/10.1371/journal.pone.0097378

Viola, A., Munari, F., Sánchez-Rodríguez, R., Scolaro, T., & Castegna, A. (2019). The metabolic signature of macrophage responses. *Frontiers in Immunology*, *10*, 1462. https://doi.org/10.3389/fimmu.2019.01462

Wizenty, J., Schumann, T., Theil, D., Stockmann, M., Pratschke, J., Tacke, F., Aigner, F., & Wuensch, T. (2020). Recent advances and the potential for clinical use of autofluorescence detection of extra-ophthalmic tissues. *Molecules (Basel, Switzerland)*, *25*(9), 2095. https://doi.org/10.3390/molecules25092095

Zhang, Q. W., Liu, L., Gong, C. Y., Shi, H. S., Zeng, Y. H., Wang, X. Z., Zhao, Y. W., Wei, Y. Q., & Hoque, M. O. (2012). Prognostic significance of tumor-associated macrophages in solid tumor: A meta-analysis of the literature. *PloS One*, *7*(12), e50946. https://doi.org/10.1371/journal.pone.0050946